Research Article

Dynamic response analysis of unbalanced rotor-bearing system with internal radial clearance

V. R. Patil[1] · P. V. Jadhav[1]

Received: 27 April 2020 / Accepted: 29 September 2020 / Published online: 15 October 2020

Abstract
This paper presents a dynamic model to predict the rotor-bearing system's vibration characteristics using Dimensional Analysis (DA). A small increment in rotor unbalance, and radial clearance can cause multiple faults, ultimately causing catastrophic failure. Hence, this model considers the influence of rotor unbalance and radial clearance on the dynamics of the rotor-bearing system. Experimental investigation reveals the effects of multiple defects at different rotor speeds. Employed Response Surface Method (RSM) correlates the clearance, unbalance, and rotor speed. Comparing experimental results with the RSM and DA indicates the effectiveness of the proposed methodology for condition monitoring of high-speed machinery in process industries.

Keywords Unbalance · Clearance · Dimension analysis (DA) · Response surface method (RSM)

1 Introduction

Rotating machinery used in processing industries is designed for high speeds, tight tolerances, and high reliability to transmit maximum power under different working conditions. The designing of such a system is necessary to maximize the equipment's life to improve its overall performance. The rotor-bearing systems of modern machinery are complex, requiring a reliable and accurate prediction of their fluctuating dynamic characteristics. The fault diagnosis and detection play an important role in the reliability of high-speed machinery [1, 2]. The vibration monitoring is gaining importance nowadays because of its accuracy and reliability. The vibration monitoring system with an advanced data acquisition system uses robust sensors and gives accurate and reliable signals widely used for early prediction of possible faults. However, the effectiveness of these systems is affected by unwanted noise and other sources of vibrations. Furthermore, the faulty rotor-bearing system exhibits multiple harmonics while running at a particular frequency. The dynamic behavior of the rotor-bearing system is affected by nonlinearities arising during operating conditions.

There are many studies carried out on the dynamic analysis of rotating machinery with different analytical models. The analytical model possesses generalization of the solution, no need for in-depth understanding, and nonessential access to the physical process for modeling. Experimental modeling possesses a high degree of accuracy within the investigational limit and more straightforward application to systems having unknown underlying physics. However, many experimental runs are often required to characterize and improve the process, which may be a costly scheme. The benefits of both are combined by a semi-analytical or semi-experimental modeling approaches such as Dimensional analysis giving high interpolative and extrapolative accuracy with few experimental runs. Since this depends on experimental data, the modeling is flexible as per the requirement of the system. Any low skilled person can perform the same with min efforts.

✉ V. R. Patil, vijaypatil872@gmail.com; P. V. Jadhav, pvjadhav@bvucoep.edu.in | [1]Mechanical Engineering Department, Bharati Vidyapeeth (Deemed To Be University) College of Engineering, Pune, India.

SN Applied Sciences (2020) 2:1826 | https://doi.org/10.1007/s42452-020-03608-y

It is reliable and straightforward as based upon physical, i.e., fundamental dimensions of the system. As cost and time are reduced compared to others, more suitable for small scale process industries are deficient with expertise in modeling, analysis, and high investment in maintenance of machines.

In a vertically supported rotor having radial clearance, the amplitude of vibration decreases as the radial clearance decreases at the critical speed [3]. Saito [4] proposed a harmonic balance methodology using Fast Fourier Transformation (FFT) for a nonlinear rotor-bearing coupling system. Ehrich [5] carried out a dynamic response analysis of a high-speed rotor system, which showed chaotic vibrations and subharmonic responses in the frequency spectrum. It gives a simple computer model based on the numerical integration of the finite difference method. Ioannis Chatzisavvas et al. [6] investigated the procedure for identifying unbalance using the equivalent load method. This procedure establishes a benchmark for the rotor at a constant speed. Krodkiewski et al. [7] formulated the nonlinear mathematical model for unbalance identification for the multi-bearing system. Tandon and Choudhury [8] developed an analytical model to predict the vibrations' amplitude and frequencies. The model forecasts the discrete spectrum amplitude and frequencies for outer and inner race defects of deep groove ball bearing under radial load conditions.

Tiwari et al. [9] showed the existence of Hopf bifurcation, sub-harmonics, and a shift in peak response through rotor-bearing experimentation. Tiwari [10] revealed the effect of stiffness on radial clearance in the horizontal rotor-bearing system. The numerically integrated system equations are validated by the harmonic balance method. Harsha [11] studied the high speed balanced horizontal rotor system's nonlinear dynamics to show the occurrence of most severe vibrations on coinciding natural frequencies with varying compliance frequency. A.S. Sekhar [12] demonstrates the vibration measurements at speed below balancing speed. It is found that modal correction mass must balance a rotor near the first critical speed with distributed unbalance. The author validates distributed unbalance in the modal balancing to balance flexible rotors having both unbalance and bow. Mohanty [13] investigated the identification of unbalance and misalignment experimentally using the model-based method. The rotor system is modeled using finite element methods, and faults modeled with equivalent loads in this method. In the equivalent load's method, the least-squares algorithm is used to identify fault parameters. This method has a limitation as parameters increases with a decrease with the number of measured vibrations. Harsha [14] investigated the nonlinear dynamics of a balanced rotor-bearing system by considering internal radial clearance. The model uses the Hertzian contact force to study the system dynamics with rotor trajectories, time response, and power spectrum. Kankar et al. [15] studied the rotor-bearing system's nonlinear dynamics for fault diagnosis by Response Surface Methodology. It is found that dynamic responses are closely related and sensitive to distributed defects and large internal clearance. Kankar et al. [16] investigated the rotor-bearing system with localized defects using Response Surface Method for fault diagnosis. The author explains the application of RSM for faults diagnosis of localized defects. Upadhyay et al. [17] studied the effects of unbalanced forces on the high-speed rotor-bearing system. The analysis was carried out at various speeds, and emphasis was given on the system's harmonic responses. The study includes the effect of combined defects on deep groove ball bearing considering Hertzian contact force and Internal Radial Clearance (IRC-C3). Lower speed transient chaos was observed. In dimensional analysis [18, 19], experimental data-based models were developed to diagnose the rotor-bearing system. The artificial neural network, regression analysis, and experimental results were used to validate the effectiveness of the models developed using dimension theory. It is claimed that the model saves time and cost of condition monitoring. However, an unbalanced rotor-bearing system with internal radial clearance was not considered in these models developed for diagnosis. Also, very few studies are reported about the dynamic analysis of an unbalanced rotor-bearing system with the internal radial clearance. The MLTθ system was used to develop the mathematical model of the system. However, a more reliable FLTθ system is used for this model. Jamadar and Vakharia [20] developed a mathematical model for bearing vibration response analysis using the Matrix Method of Dimensional Analysis (MMDA). The model was validated using RSM and experimental results. A lot of research is directed towards the fault diagnosis of the rotor-bearing systems with different methods and faults. Many researchers carried research on fuzzy logic; neural networks. However, the success of these techniques depends on how fault features are extracted from the system. Hence, an attempt has been made to investigate the dynamic response analysis of an unbalanced rotor-bearing system with loosely fitted bearing by providing artificial internal radial clearance.

The literature review revealed that the effects of clearance and unbalance had not been studied using Dimensional Analysis (DA). Hence, this inspires to the investigation of an unbalanced rotor-bearing system's vibration response having internal radial clearance by using DA and RSM. In this work, the vibration amplitude and defect frequency are predicted using the DA method based on Buckingham's pi theorem. The results of DA are compared with experimental and RSM results. In the rest of

the paper, mathematical expressions are derived in Sect. 2 and 3. Section 4 and 5 present the experimental analysis and Response Surface Methods followed by results. The detailed results and discussion are given in Sect. 6 and followed by the conclusions in Sect. 7.

2 Dynamic model of the rotor-bearing system

A new dimensional analysis approach to model physical problems in simple form is applied to develop a mathematical model. The mathematical model is developed to estimate the amplitude of vibration using Dimensional Analysis (DA) techniques. In the dimensional analysis, the first task is to identify the process parameters. The process parameter involves independent variables, dependent variables, and extraneous variables.

As per the dimension theory, the "complete" set of the parameters may consist of dependent variables obtained from other variables, and none of the independent variables are derived from other variables [21]. The independent variables involve rotor-bearing geometry, material properties, and operating conditions.

A set of variables for establishing a mathematical model to obtain dynamic behavior is presented in three basic dimensions—length L, time T, and force F [21, 22]. Figure 1 shows the correlation between the variables affecting the dynamic behavior of the system. Table 1 shows variables of the system with their corresponding dimensions, symbol, and unit system.

According to the dimensional analysis [21, 22], a complete set of dimensionless products consists of total variables besides the maximum variables that will not form a dimensionless product. In the proposed model, vibration amplitude (dependent variable) can be expressed in other parameters given in Eq. (1). '*f*' is the unknown function and represents the relation between input variables and experimentally obtained response variables.

$$V = f\left(D, d_b, d_i, d_o, d_m, B, L, \rho, E_S, E_R, W_s, W_r, I_s, I_r, c, \delta, T, \Delta, f_s\right) \quad (1)$$

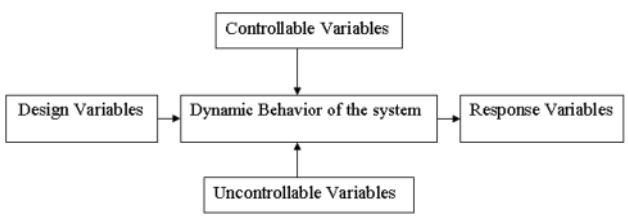

Fig. 1 Variable affecting on the dynamic behavior of the system

In the rotor-bearing system, the unbalanced mass, clearance, and speed of rotation play a significant role in changing the dynamic behavior of the system, therefore in this model, the effect of unbalanced mass, clearance, and speed of rotation on the amplitude of vibration of the rotor-bearing system bearing is considered. All the above variables considered for the formulation of the mathematical model are expressed as the number of dimensionless products as given in Eq. (2)

$$f\left(\pi_1, \pi_2, \pi_3, \ldots., \pi_m\right) = 0 \quad (2)$$

The total number of the dimensionless product is 23, and 03 variables do not form dimensionless products, as reported in Table 1. As per the applied dimensional analysis and modeling [21, 22], 23–3 = 20 parameters are required to describe the complete set.

Table. 1 Parameter for modeling the dynamic response of the system

Parameter	Symbol	Unit	Dimension
Inner race diameter	d	mm	L
Ball diameter	d_b	mm	L
Pitch diameter	d_1	mm	L
Bearing Width	B	mm	L
Length of shaft	L	mm	L
No. of Balls	Z	–	–
Density of bearing	ρ	$\frac{kg}{m^3}$	$FL^{-4}T^2$
Young's Modulus	E	$\frac{N}{mm^2}$	FL^{-2}
Contact force for deformation	k	$\frac{N}{mm^{1.5}}$	$FL^{-1.5}$
Hertzian contact force	F_h	N	F
Mass of shaft	m_s	Kg	FL^2
Mass of rotor	m_r	Kg	FL^2
Mass Moment of Inertia of Shaft	I_s	$Kg.mm^2$	FL^2
Mass Moment of Inertia of Rotor	I_r	$Kg.mm^2$	FL^2
Damping factor	c	$\frac{Ns}{m}$	$FL^{-1}T^1$
Speed of shaft	N	rpm	T^{-1}
Radial load	T	N	F
Bearing deflection	δ	mm	L
Unbalance mass on rotor	W_u	Kg	$FL^{-1}T^2$
Internal radial clearance	R_c	μm	L
Lubricant viscosity	υ	mm^2/s	L^2T^{-1}
Vibration amplitude	V	$\frac{mm}{s}$	LT^{-1}
Varying frequency component	F_{vc}	Hz	T^{-1}
Inner race defect frequency	f_{bpf}	Hz	T^{-1}
Unbalance defect frequency	f_u	Hz	T^{-1}

3 Rotor-Bearing Model

The functional dependence of vibration characteristics is obtained from the association of the theory of dimensional analysis and Buckingham's 'π' theorem. The pitch diameter, speed of the shaft, and radial load are taken as repeating variables. These three variables are not going to form a dimensionless group [21, 22]. The dynamic response model can be written as

$$\pi_R = V\left[d_1\right]^a [N]^b [W]^c \tag{3}$$

where a, b, and c represents constants, obtained from fundamental units, as given in Eq. (4).

$$\pi_R = LT^{-1}[L]^a \left[T^{-1}\right]^b [F]^c \tag{4}$$

The balancing of the fundamental units to find constants a, b, and c, may be done as

$$F^0L^0T^0 = F^cL^{1+a}T^{-b-1} \tag{5}$$

The equations may be written as follows

$$c = 0$$

$$1 + a = 0$$

$$-b - 1 = 0$$

By solving the above equations, the unknowns can be obtained as

$$a = -1$$

$$b = -1$$

$$c = 0$$

Therefore, the first dimensionless group expressed as

$$\pi_R = V\left[d_1\right]^{-1}[N]^{-1}\left[W_u\right]^0$$

$$\pi_R = \frac{V}{d_1 N} \tag{6}$$

With a similar procedure, the remaining 20 dimensionless groups are obtained and are listed in Table 2.

3.1 Deducing of dimensionless groups

As the numbers of dimensionless variables are more, it is required to reduce these dimensionless groups. The reduction is carried out by taking products or divisions of one group by another group. They are reduced by performing the following mathematical operations:

Table 2 Dimensionless Variables

variable	π-terms	variable	π-terms
d_1, N, W, and V	$\pi_R = \frac{V}{d_1 N}$	d_1, N, W, and ρ	$\pi_8 = \frac{\rho d_1^4 N^2}{W}$
d_1, N, W, and d_b	$\pi_1 = \frac{d_b}{d_1}$	d_1, N, W, and K	$\pi_9 = \frac{K d_1^{1.5}}{W}$
d_1, N, W, and B	$\pi_2 = \frac{B}{d_1}$	d_1, N, W, and δ	$\pi_{10} = \frac{\delta}{d_1}$
d_1, N, W, and L	$\pi_3 = \frac{L}{d_1}$	d_1, N, W, and F_H	$\pi_{11} = \frac{F_H}{W}$
d_1, N, W, and Z	$\pi_4 = Z$	d_1, N, W, and C	$\pi_{12} = \frac{C N d_1}{W}$
d_1, N, W, and E	$\pi_5 = \frac{E d_1^2}{W}$	d_1, N, W and R_c	$\pi_{13} = \frac{R_c}{d_1}$
d_1, N, W and I_s	$\pi_6 = \frac{I_s}{W d_1^2}$	d_1, N, W, and Wu	$\pi_{14} = \frac{Wu d_1 N^2}{W}$
d_1, N, W and I_s	$\pi_7 = \frac{I_r}{W d_1^2}$	d_1, N, W, and υ	$\pi_{15} = \frac{\upsilon}{N d_1^2}$

$$\pi_a = \frac{\pi_6 \times \pi_7}{\pi_1 \times \pi_2 \times \pi_3} \qquad \pi_b = \pi_{14}$$

$$\pi_c = \frac{\pi_2}{\pi_5} \times \pi_8 \times \pi_{13} \qquad \pi_d = \frac{1}{\pi_9 \times \pi_{15}}$$

$$\pi_a = \frac{\pi_6 \times \pi_7}{\pi_1 \times \pi_2 \times \pi_3}$$
$$\pi_a = \frac{I_s I_r}{W^2 d_1 d_b B L} \tag{7}$$

$$\pi_b = \pi_{14}$$
$$\pi_b = \frac{W u d_1 N^2}{W} \tag{8}$$

$$\pi_c = \frac{\pi_2}{\pi_5} \times \pi_8 \times \pi_{13}$$
$$\pi_c = \frac{\rho B R_c N^2}{E} \tag{9}$$

$$\pi_d = \frac{1}{\pi_9 \times \pi_{15}}$$
$$\pi_d = \frac{W d_1^{.05} N}{k \upsilon} \tag{10}$$

From above dimensionless variables, $(\pi_{10}, \pi_{11}, \pi_{12})$ form a constant dimensionless group (Ψ) can be written as,

$$\Psi = (\pi_{10} \times \pi_{11} \times \pi_{12}) \tag{11}$$

where Ψ the group of the dimensionless variables remains constant during the experimentation.

Using Eq. (11), π_1 maybe written as,

$$\pi_R = f\left(\Psi, \pi_a, \pi_b, \pi_c, \pi_d\right) \tag{12}$$

Substituting above dimensionless group, the Eq. (12) may be obtained as follows

$$\pi_R = f\left(\Psi\frac{l_s l_r}{W^2 d_1 d_b B L}\times\frac{Wud_1N^2}{W}\times\frac{\rho BR_cN^2}{E}\times\frac{Wd_1^{0.5}N}{k\upsilon}\right) \quad (13)$$

Hence, a total of 20 parameters involved in the problem have been reduced to five dimensionless parameters. The relationship in the above governing equation can be written as [21, 22]

$$\pi_R = \Psi\times(\pi_a)^{a1}\times(\pi_b)^{a2}\times(\pi_c)^{a3}\times(\pi_d)^{a4} \quad (14)$$

The governing Eq. (13) is solved by multiple factorial regression [23] using a code developed in MATLAB software, and the coefficients a0, a1, a2, a3, a4 are obtained by following the process of [23] as -

$$\pi_R = 0.091\pi_e\times^{-0.9103}\times\pi_j^{-1.7925}\times\pi_k^{0.26135}\times\pi_{20}^{0.1379} \quad (15)$$

Similarly, other equations for the defect frequency can be developed.

$$\pi_F = 0.075\pi_e\times^{0.478}\times\pi_j^{1.235}\times\pi_k^{-0.167}\times\pi_{20}^{-0.1524} \quad (16)$$

Equation (15) and (16) show the vibration amplitude and defect frequency predictions model, respectively. The flow chart for the proposed methodology is shown in Fig. 2.

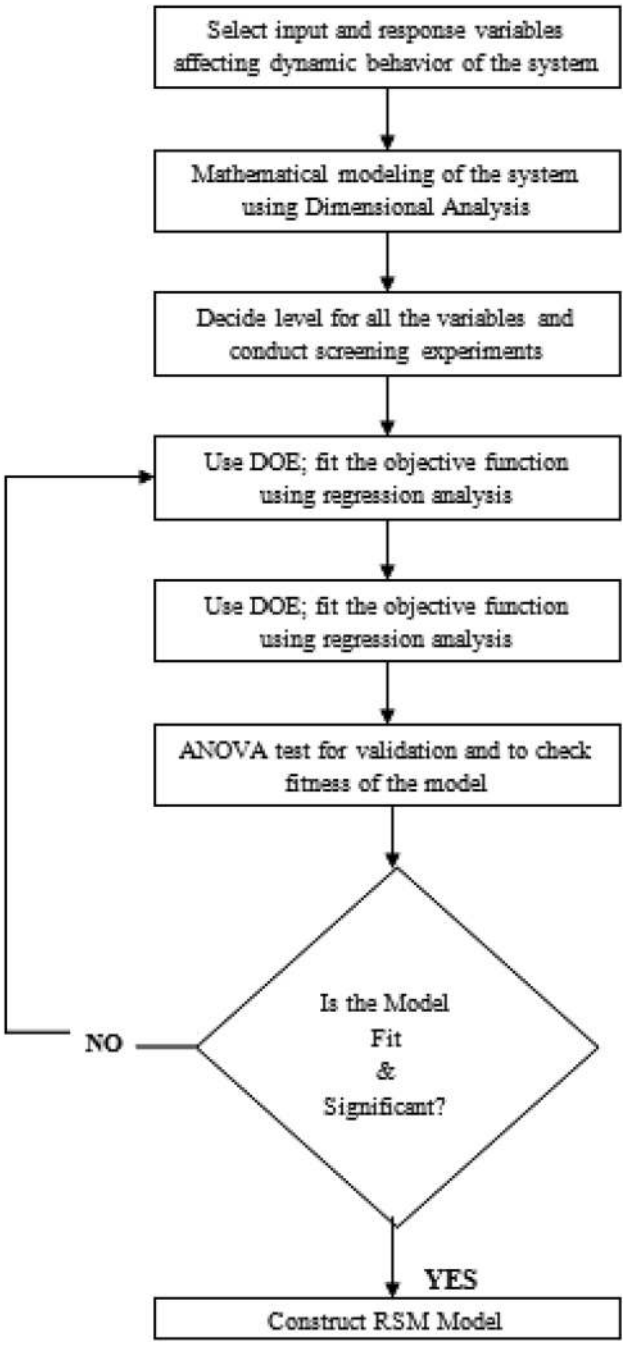

Fig. 2 Flow chart of the methodology

4 Experimental system

Figure 3 shows the schematic layout of the experimental setup. It consists of a rotor shaft supported on two bearings. The AC motor drives this through the flexible coupling. The AC motor is connected with the variable frequency drive, and the controller unit is used to drive the shaft at various speeds. The bearing housing is fixed on the support frame. The two deep groove ball bearings, 6209/C3-SKF (Sweden), are used. The specifications of the bearing are given in Table 3. The characteristic defect frequencies are given in Table 4. The SKF LGMT3 type grease is used for the lubrication of the bearing. The accelerometer (ADASH piezoelectric type-1A-AC101, sensitivity-100 mV/g) with the Fast Fourier transform (FFT) analyzer is used to measure its vibration responses. The bearing's stiffness is obtained by testing bearing on the universal testing machine with a proper fixture. The damping is obtained by conducting an impact hammer test by using an FFT analyzer. The mass of the rotor and mass of the shaft is approximately 3 kg and 5 kg, respectively. The experiments have been performed by adding an unbalanced mass approximately equal to 3% and 4% of the rotor's mass. The artificial internal radial clearance is created in the bearing and shaft. The internal radial clearance of 0.04 mm and 0.02 mm is maintained between the shaft, and the sleeve of bearing and clearance of 0.04 mm and 0.02 mm is maintained between the inner race and the sleeve of the bearing, respectively, by losing the lock nut as shown in Figs. 4 and 5. The feeler gauge is used to measure internal radial clearance. The accelerometer is placed on the test bearing, as shown in Fig. 3. Variation in

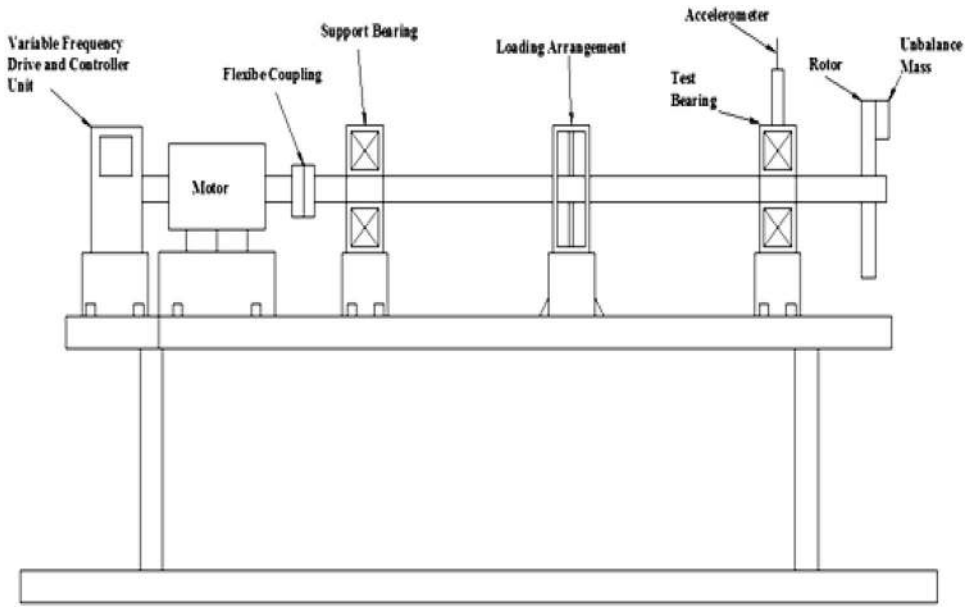

Fig. 3 Schematic layout of the experimental setup

Table 3 Rotor-bearing system specifications

Rolling element bearing	SKF 6209
Outer race diameter (do)	85 mm
Inner race diameter (di)	45 mm
Ball diameter (db)	9 mm
Bearing Width (B)	19 mm
Radial load (T)	2500 N
Rotor disc diameter (dr)	180 mm
Mass of rotor, (Wr)	3 kg
Mass of the shaft, (Ws)	5 kg

Table 4 Deterministic characteristic defect frequencies of the system

Frequency components (Hz)	Expressions	Shaft Speed	
		1000	2500
f_{FTF}	$\frac{1}{2}\frac{N}{60}\left(1-\frac{d_b}{d_1}cos\theta\right)$	7.17	17.94
f_{VCF}	$Z \times fFTF$	64.53	161.46
F_{BPFI}	$\frac{Z}{2}\frac{N}{60}\left(1+\frac{d_b}{d_1}cos\theta\right)$	85.34	213.46
F_{BPFO}	$\frac{Z}{2}\frac{N}{60}\left(1-\frac{d_b}{d_1}cos\theta\right)$	64.58	161.53

the unbalance and internal radial clearance is simulated on the experimental set up between 1000 and 2500 rpm to obtain the dynamic response.

Fig. 4 Clearance of 0.04 mm in the shaft and sleeve

Fig. 5 Clearance of 0.02 mm in the sleeve and Inner race

The vibration response spectra for all cases are presented in the frequency domain. The Response Surface Method (RSM) investigates the correlation between variables and their interactions. The results are compared with the results obtained through the dimensional analysis approach.

with three variables and 2 levels, a total of 8 experiments are designed to obtain vibration amplitude and defect frequencies. Table 5 gives the details of the design of experiments.

5 Response surface method (RSM)

The RSM is a mathematical and statistical tool used for model responses of systems. The extraction of data affects the prediction of the model's dynamic response and, hence, the selection of proper sampling size is important. As per the Taguchi technique, 8 trial runs are designed using Minitab-16. Details of trial runs are reported in Table 6. The RSM has been used for studying the influence of three parameters (speed, clearance, and unbalanced mass) on different responses of the rotor-bearing system. The relation between dependent and independent variables is expressed as

$$A = \beta_0 + \beta_1 a_i + \beta_2 b_i + \cdots + \beta_n f_n + e_i$$

where 'A' is the dependent variable, ie. Response amplitude and '*i*' is the no. of the experiments and $a_i, b_i, \ldots, f_n$ represents the independent variable are given below.

$$a_i = R_c,\ \ b_i = N_r,\ c_i = W_u,\ d_i = R_c \times W_u,$$

$$e_i = R_c \times N,\ f_i = W_u \times N$$

The $\beta_0, \beta_1, \beta_2, \ldots \beta_n$ are constants and e_i represents the error between them [24]. The repeated experiments were conducted in experimental data analysis for better evaluation of error. The Minitab-16 is used to analyze the experimental data and response variables. Response amplitude peak and defect frequency values are given in Table 6 for various combinations of radial clearance, speed, and unbalanced masses.

Table 5 Levels of the variables of experimental design

Variables	Design variables	Levels	
		1	2
Radial clearance	Rc (mm)	0.02	0.04
Speed	N (rpm)	1000	2500
Unbalance mass	Wu (kg)	0.084	0.120

Table 6 Taguchi method planning for obtaining response amplitude and defect frequency

Trial No	1	2	3	Response amplitude peak (mm/s)	Defect frequency (Hz)
1	0.02	1000	0.084	0.362	17
2	0.02	2500	0.084	0.446	34
3	0.04	2500	0.12	0.851	34
4	0.04	1000	0.12	0.635	34
5	0.04	2500	0.084	0.491	38
6	0.04	1000	0.084	0.597	17
7	0.02	2500	0.12	0.627	33
8	0.02	1000	0.12	0.421	17

6 Results and discussion

Vibration amplitude and defect frequencies are calculated using developed dimensional analysis model expression Eq. (15). The frequency response plot obtained experimentally for all 8 trials is shown in Figs. 6, 7, 8, 9, 10, 11, 12 and 13. The results of each trial are discussed below:

Trial 1 - This trial is conducted with a clearance of 0.02 mm, an unbalanced mass of 0.084 kg, and a shaft speed of 1000 rpm. The frequency response plot is shown in Fig. 6. The significant peak at a frequency of 1× rpm and 0.362 mm/s amplitude is observed. Also, the vibration excitation is observed at multiple frequencies of rotation. Other peaks are observed at fundamental train frequency f_{FTF} equal to 8 Hz, the combinations of ball pass frequency of the inner race and shaft as $f_{BPFI} + 1.5\ f_{FTF}$ equal to 98 Hz. Other frequency components such as combinations of ball

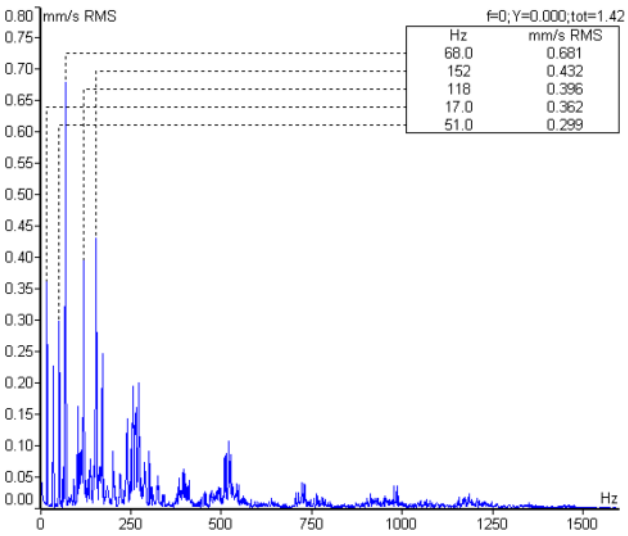

Fig. 6 Frequency response plot for trial 1

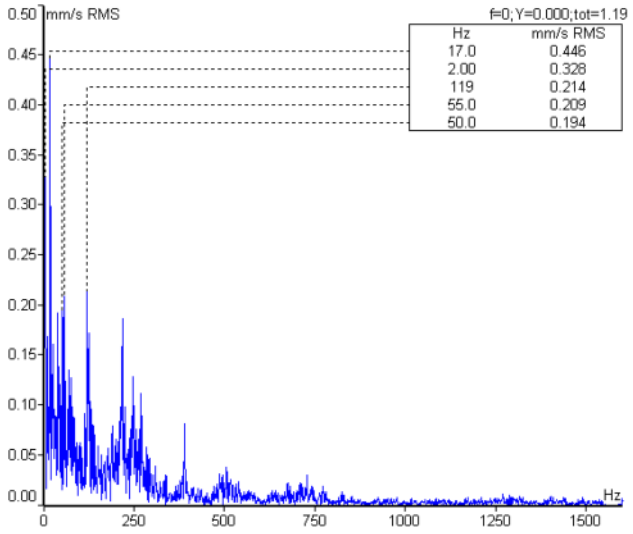

Fig. 7 Frequency response plot for trial 2

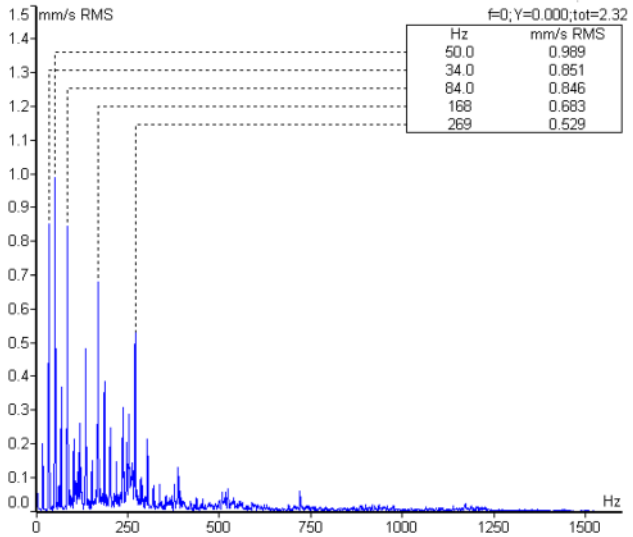

Fig. 8 Frequency response plot for trial 3

pass frequency of the inner race and shaft as $f_{BPFI} + 4.5\ f_{FTF}$ equal to 125 Hz and 2.94 f_{BPFI} of 250 Hz can be observed. The experimental values closely match with predicted values.

Trial 2 - This trial is conducted with a clearance of 0.02 mm and an unbalanced mass of 0.084 kg. Shaft speed is 2500 rpm. The frequency response plot is shown in Fig. 7. The significant peak at a frequency of 1/3× pm and 0.446 mm/s amplitude is observed. The vibration excitation is observed at multiple of sub-harmonics frequencies of rotation. The other essential peak observed at multiples of rotation frequency 3× rpm equal to 50 Hz. The experimental value closely matches with predicted values. The peaks obtained by FFT at multiples of rotation frequency closely matches with a model derived from the dimensional analysis.

Trial 3 - This experiment is conducted with a clearance of 0.04 mm and an unbalanced mass of 0.120 kg. Shaft speed is 2500 rpm. The frequency response plot is shown in Fig. 8. In this trial, multiples of sub-harmonics frequencies of rotation are seen, and maximum peak at a frequency of 1/3× rpm of 0.851 mm/s amplitude is observed. The combined fault leads to an increase in the overall vibration level. It is also found that as clearance increases, the amplitude of vibration increases as the square of the shaft's running speed. The other significant peak at f_{BPFI} equal to 268 Hz can be observed.

Trial 4 - This experiment is conducted with a clearance of 0.04 mm and an unbalanced mass of 0.120 kg. Shaft speed is 1000 rpm. The frequency response plot is shown in Fig. 9. In this trial, multiples of sub-harmonics frequencies of rotation are seen, and maximum peak at a frequency of 1/3× rpm of 0.635 mm/s amplitude is observed. It is seen that highly unbalanced forces and speed increase the vibration level of the system. Also, it is seen that system is unstable because of high unbalanced forces. The other significant peak at f_{BPFI} equal to 72 Hz can be observed.

Trial 5 - This experiment is conducted with a clearance of 0.04 mm and an unbalanced mass of 0.084 kg. Shaft speed is 2500 rpm. The frequency response plot is shown in Fig. 10. In this trial, the second-order spectrum with harmonics in nature with a peak of 0.491 mm/s amplitude is seen. Significant peaks are observed at 1× rpm and 2× rpm harmonics. It is found that as radial clearance increases, the amplitude of vibration increases.

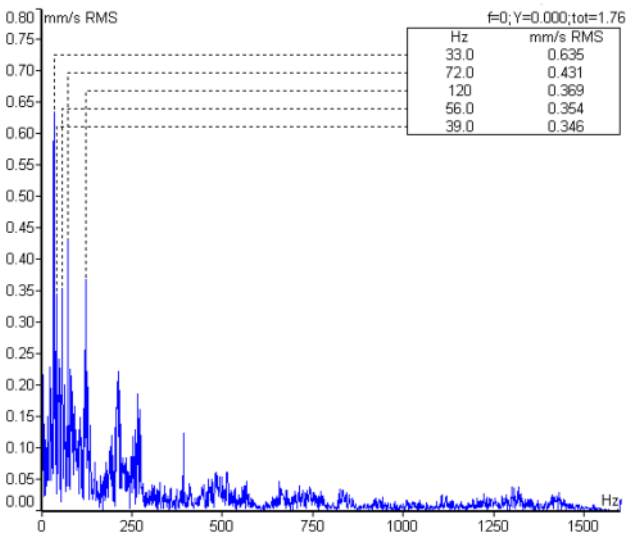

Fig. 9 Frequency response plot for trial 4

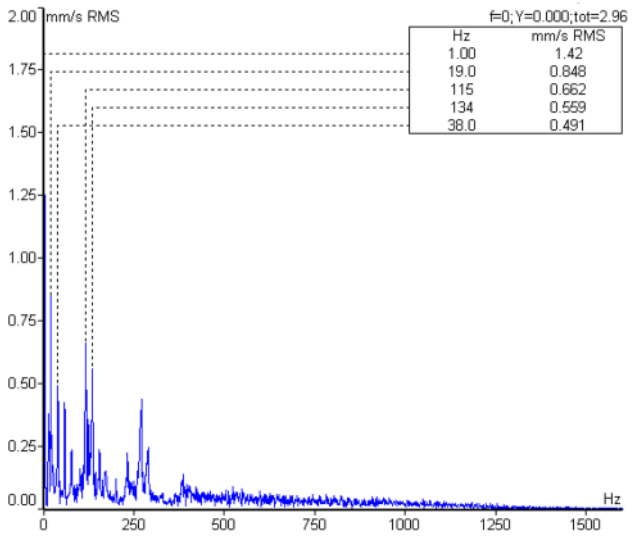

Fig. 10 Frequency response plot for trial 5

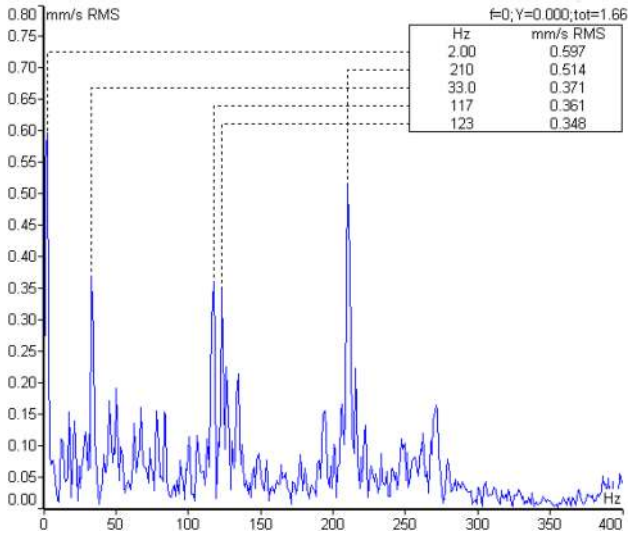

Fig. 11 Frequency response plot for trial 6

Trial 6 - This experiment is conducted with a clearance of 0.04 mm and an unbalanced mass of 0.084 kg. Shaft speed is 1000 rpm. The frequency response plot is shown in Fig. 11. In this trial, the second-order spectra with harmonics with a peak of 0.591 mm/s amplitude are observed at sub-harmonics frequencies of rotation. The other significant peak at f_{BPFI} equal to 210 Hz can be observed.

Trial 7 - This experiment is conducted with a clearance of 0.02 mm and an unbalanced mass of 0.084 kg. Shaft speed is 2500 rpm. The frequency response plot is shown in Fig. 12. In this trial, the second-order spectra with harmonics in nature are observed.

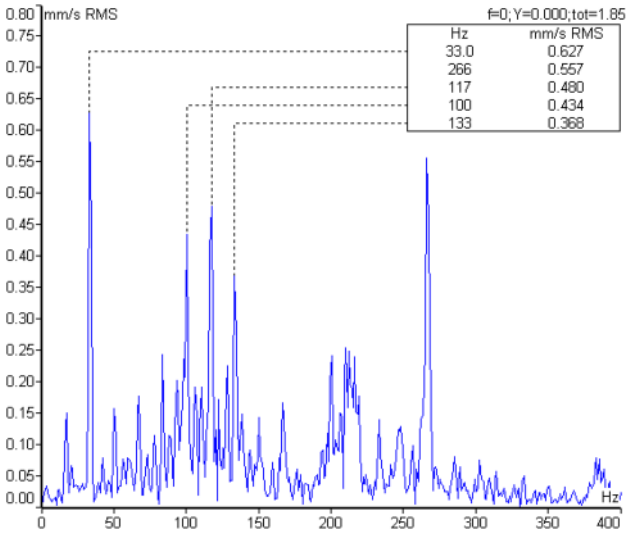

Fig. 12 Frequency response plot for trial 7

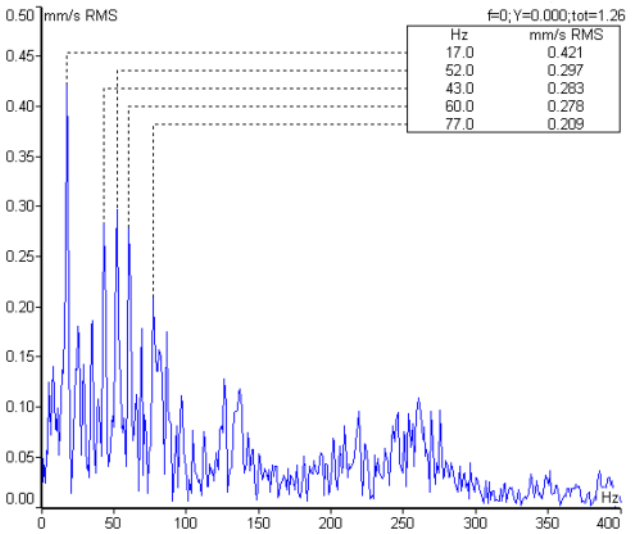

Fig. 13 Frequency response plot for trial 8

Trial 8 - This experiment is conducted with a clearance of 0.02 mm and an unbalanced mass of 0.120 kg. Shaft speed is 1000 rpm. The frequency response plot is shown in Fig. 13. In this trial, second-order spectra with harmonics in nature are observed.

The system's chaos is observed from the above trial with the increase in peak amplitude of vibration. It indicates that at higher values of unbalance mass and clearance

Table 7 Comparison of numerical and experimental results

Trial no	Vibration amplitude (mm/s), Frequency in (Hz)	
	Model	Experiment
1	**(0.3695, 17)**	(0.362, 17)
2	**(0.4486, 34)**	(0.446, 34)
3	**(0.8447, 34)**	(0.851, 34)
4	**(0.6340, 34)**	(0.635, 34)
5	**(0.489, 38)**	(0.491, 38)
6	**(0.5923, 17)**	(0.597, 17)
7	**(0.6319, 34)**	(0.627, 33)
8	**(0.4239, 17)**	(0.421, 17)

Bold values indicate significant value of particular factor

Table 8 ANOVA for response amplitude, clearance, speed and unbalance mass

Source	DF	SS	MS	F	P
Main Effect	3	0.093548	0.031183	4681.18	0.011
Clearance	1	0.053350	0.053350	8009.02	**0.007***
Speed	1	0.031413	0.031413	4715.74	**0.009***
Unbalanced mass	1	0.008785	0.008785	1318.78	**0.018***
Interaction	3	0.000909	0.000303	45.47	0.108
$R_c \times W_u$	1	0.000668	0.000668	100.27	0.063
$R_c \times N$	1	0.000067	0.000067	10.01	0.195
$W_u \times N$	1	0.000174	0.000174	26.11	0.123
Error	1	0.000007	0.0000007		
Total	7	0.094463			
$R^2 = 99.99\%$	R^2-(adj) = 99.95%				

*Indicates significant factor

increases the vibration level of the system. Also, combined faults harmonics are seen at 1× rpm and 1/3× rpm of speed. From the above trial, it is clear that vibration excitation is observed at multiple frequencies of rotation and 1/3× of sub-harmonics of frequencies.

From the result analysis of trial 1 to trial 8, it is clear that the peak amplitude and defect frequencies obtained through the experimental study closely matches with the values predicted by the model Eq. 15.

The values of the amplitude of vibration and defect frequencies predicted by the mathematical model and experimental results are shown in Table 7. The numerical results and experimental results show good agreement for all 8 trial runs. The Minitab-16 software has been used to analyze the experimental data and analysis of variance (ANOVA). Regression coefficients at 5% confidence have been obtained. The *p* values and regression coefficients are reported in Table 8. It shows that a p-value of less than 0.05 indicates the significance of the factor [23].

ANOVA is performed to analyze the results and interaction effect of the variables. Results obtained through ANOVA are listed in Table 8.

The *f* value 4681.18 indicates that the polynomial regression equation is significant. From ANOVA, it is observed that internal radial clearance, speed, and unbalanced mass are the significant parameter which affects vibration amplitude. The response surface plots for clearance and unbalanced mass vibration amplitude is shown in Fig. 14a–c.

The relationship between vibration and speed amplitude is shown in surface response Fig. 14a. It is clear that as speed increases, the amplitude of vibration also increases. Also, the unbalance mass has a significant effect on response amplitude. Figure 14b shows that as radial clearance increases, the amplitude of vibration increases. Figure 14c also shows that unbalanced mass and clearance significantly affect the vibration amplitude. The polynomial regression is solved to obtain vibration amplitude as given below.

$$\text{Response amplitude peak (mm/s)} = 0.5282 + 0.08166\, \boldsymbol{a_i} + 0.06266\, \boldsymbol{b_i} + 0.003314\, \boldsymbol{c_i} + 0.009121\, \boldsymbol{d_i} - 0.002872\, \boldsymbol{e_i} + 0.004622\, \boldsymbol{f_i} \quad (17)$$

Equation (17) is used to obtain response amplitude with clearance and unbalance defect condition.

The comparison of vibration amplitude obtained for all 8 trial runs by experimental analysis, numerical results obtained by DA, and RSM are shown in Fig. 15. Results predicted by the mathematical model, experimental results, and RSM values match and reveal that the proposed model is reliable for diagnosing the rotor-bearing system.

The comparison of results with experimentation confirms the usefulness and accuracy of the RSM and DA. The results indicate that the proposed model forms an efficient approach to predicting the rotor-bearing system's dynamic behavior under unbalance and internal radial clearance conditions. This dimensional analysis approach can be easily implemented for condition monitoring.

7 Conclusion

This work demonstrates the dynamic modeling of the rotor-bearing system using DA to predict its vibration characteristics. Small enhancements in the rotor unbalance and radial clearance tends to develop multiple faults or turn into complete system failure. Hence, the present modeling considers the effect of the rotor unbalance and radial clearance on the rotor-bearing system's vibration response. The developed MATLAB code solves

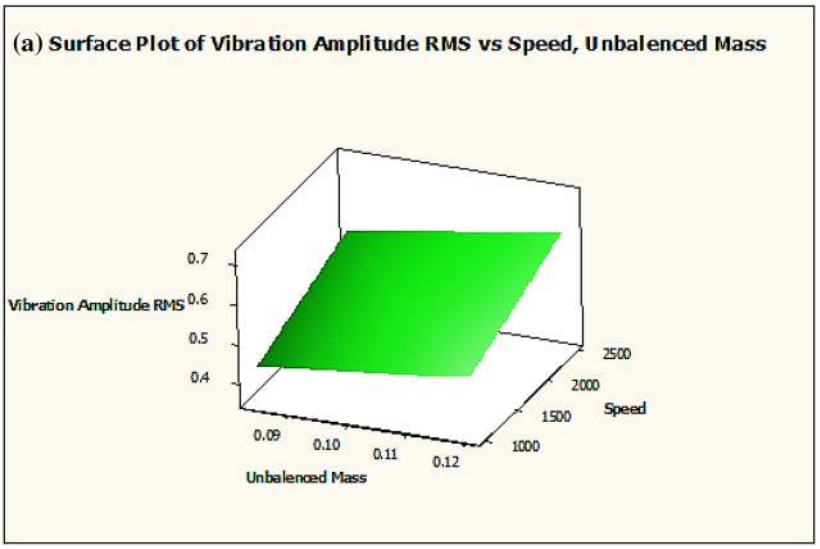

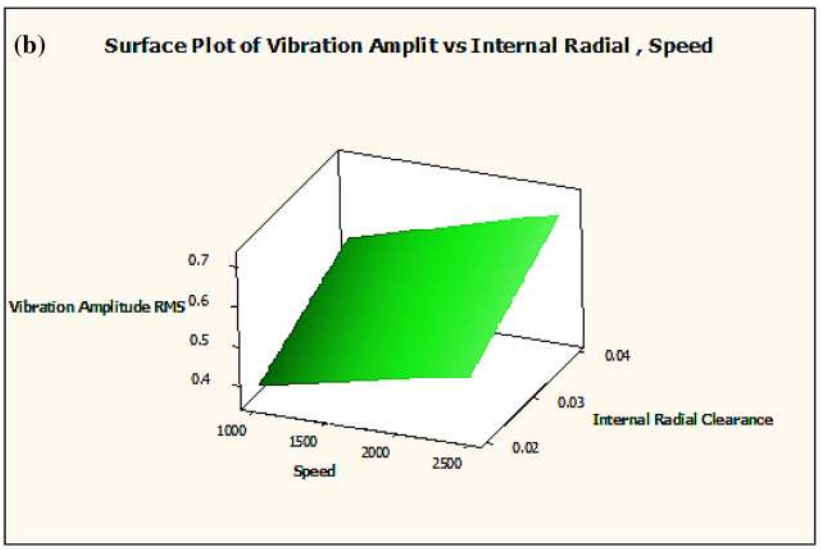

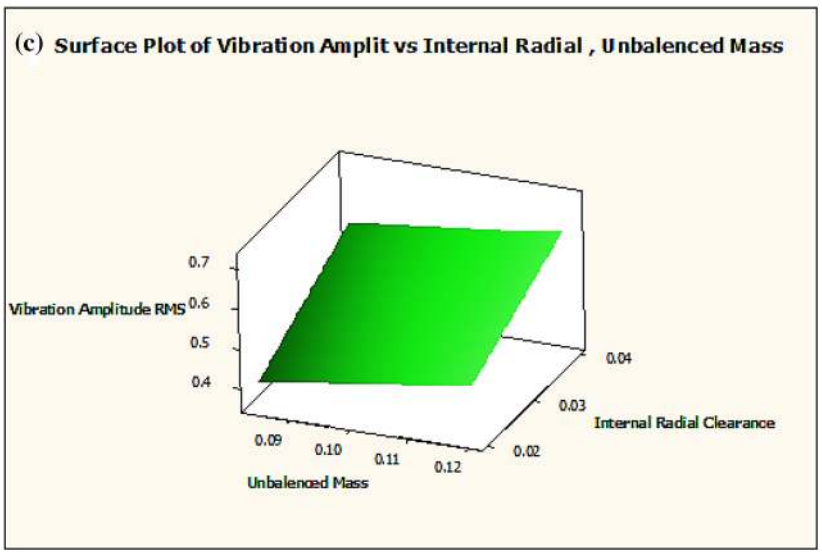

Fig. 14 **a** Surface plots for response amplitude (mm/s RMS), unbalanced mass (kg) and speed (rpm), **b** Surface plots for response amplitude (mm/s RMS), speed (rpm), and internal radial clearance (µm), **c** Surface plots for response amplitude (mm/s RMS), unbalanced mass (kg) and internal radial clearance (µm)

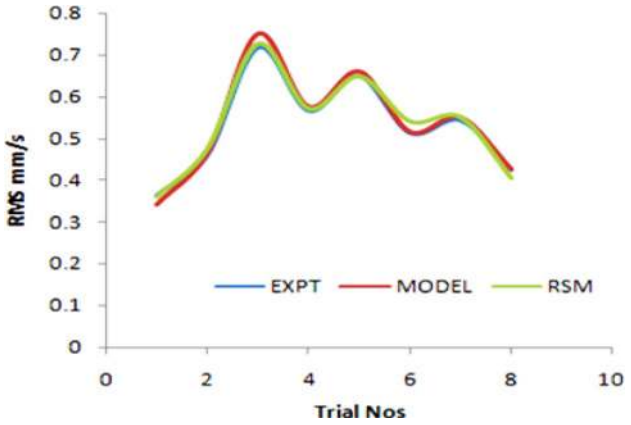

Fig. 15 Comparison of vibration amplitude with the number of experiments

the mathematical equations, and the steady-state solutions are sought for different amplitudes and frequencies. Experimentation was performed to obtain the vibration response of the developed test setup under different faults such as unbalance and radial clearance. The Response Surface Method (RSM) is used to investigate the dependency of unbalanced mass, speed, and clearance on the response parameters, i.e., vibration amplitude and defect frequencies.

Theoretical bearing defect frequencies are in good agreement with those obtained experimentally. Also, obtained vibration characteristics such as amplitude and defect frequencies are close matches with DA results. DA model allows determining the effect of faults such as unbalance and internal radial clearance. It is seen that the amplitude of vibration significantly affected under the variation in the rotor speed, internal radial clearance, and unbalance mass and ultimately changes the nonlinear system's dynamic response. Also, rotor speed and internal radial clearance were found dominant between the system's response parameters. The change in system response is linear at lower clearance levels, unbalanced mass, and rotor speed. Whereas, the chaos is observed at a higher level of the operating parameters. The significant peaks occur at a rotational frequency of 1× rpm and multiple sub-harmonics frequencies of rotation for combined faults. The internal radial clearance found the most significant factor affecting the system's vibration response from the surface response plot. Good agreement is observed among mathematical models, experimental results, and RSM results. This study contributes to the condition monitoring of high-speed machinery in the sugar, food, and power industries. The rotor unbalances, and radial clearance effect can be investigated under fluctuating load and rotor speed in future studies.

Compliance with ethical standard

Conflict of interest On behalf of all authors, the corresponding author states that there is no conflict of interest.

References

1. Childs MD (1993) Turbomachinery Rotordynamics. Wiley, Chichester
2. Ehrich FF (1992) Handbook of Rotordynamics. McGraw-Hill, New York
3. Yamamoto T (1955) On the vibration of a shaft supported by bearings having radial clearances. Trans JSME 21:182–192
4. Saito S (1985) Calculation of nonlinear unbalance response of horizontal Jeffcott rotors supported by ball bearings with radial clearances. ASME J Vib Acoust Stress Reliab Design 107:416–420
5. Ehrich FF (1988) Higher-order sub-harmonic response of high-speed rotors in bearing clearance. ASME J Vib Acoust Stress Reliab Design 110:9–16
6. Chatzisavvas I, Dohnal F (2015) Unbalance identification using the least angle regression technique. Mech Syst Signal Process 50:706–717
7. Krodkiewski JM, Ding J, Zhang N (1994) Identification of unbalance change using a nonlinear mathematical-model for multi bearing rotor systems. J Sound Vib 169:685–698
8. Tandon N, Choudhury A (1997) An analytical model for the prediction of the vibration response of rolling element bearings due to a localized defect. J Sound Vib 205(3):275–292
9. Tiwari M, Gupta K, Prakash O (2000) Dynamic response of an unbalanced rotor supported on ball bearings. J Sound Vib 238:757–779
10. Tiwari M, Prakash O, Gupta K (2000) Effect of radial internal clearance of a ball bearing on the dynamics of a balanced, horizontal rotor. J Sound Vib 238(5):723–756
11. Harsha SP, Sandeep K, Prakash R (2003) The effect of speed of balanced rotor on nonlinear vibrations associated with ball bearings. Int J Mech Sci 47(4):225–240
12. Deepthikumar MB, Sekhar AS, Srikanthan MR (2013) Modal balancing of flexible rotors with bow and distributed unbalance. Elsevier J Sound Vib 332:6216–6233
13. Jalan AK, Mohanty AR (2009) Model based fault diagnosis of a rotor bearing system for misalignment and unbalance under steady-state condition. J. Sound Vib 327: 604–622.
14. Harsha SP (2006) Nonlinear dynamic response of a balanced rotor supported by rolling element bearings due to radial internal clearance effect. Mech Mach Theory 41:688–706
15. Kankar PK, Harsha SP, Pradeep K, Sharma SC (2009) Fault diagnosis of a rotor-bearing system using response surface method. Eur J Mech A Solids, Elsevier publishers 28(2009):841–857
16. Kankar PK, Sharma SC, Harsha SP (2011) Fault diagnosis of high-speed rolling element bearings due to localized defects using response surface method. ASME J Dyn Syst Meas Control 133(2):031007
17. Yadav H, Upadhyay SH, Harsha SP (2013) Study of effect of unbalanced force for high-speed rotors. Procedia Eng (Elsevier Publisher) 64(2013):593–602
18. Desavale RG, Kanai RA, Venkatachalam R, Chavan SP, Jadhav PM (2015) Vibration characteristics diagnosis of roller bearing using the new empirical model. ASME J Tribol 138(1):011103
19. Desavale RG (2018) Dynamics characteristics and diagnosis of a rotor-bearing's system through a dimensional analysis approach: an experimental study. ASME J Comput Nonlinear Dyn 14(1):014501

20. Jamadar IM, Vakharia DP (2016) A numerical model for the identification of the structural damages in rolling contact bearings using matrix method of dimensional analysis. ASME J Tribol 138(2):021106
21. Langhaar HL (1951) Dimensional analysis, and theory of models. Wiley, New York
22. Gibbings JC (2011) Dimensional analysis. Springer, London Ltd
23. John OR, Sastry GP, David AD (1998) Applied regression analysis—a research tool, 2nd edn. Springer, New York
24. Raymond HM, Douglas CM, Christine MAC (2009) Response surface methodology, 3rd edn. Wiley, India